# RADIATIVE TRANSFER MODELLING FOR CALIBRATION AND ATMOSPHERIC CORRECTION

E. VERMOTE AND J.C. ROGER
*NASA / Goddard Space Flight Center,*
*Greenbelt, MD, 20771,*
*U.S.A.*

ABSTRACT. The remotely-sensed signals in the visible and near infrared channels at satellite or airborne platforms are combinations of surface and atmospheric contributions, with relative amounts varying across the two wavelength regions, depending on the condition of the atmosphere. In order to derive accurate sensor calibration and atmospheric correction, the contribution of the atmospheric constituents to the total retrieved signal must be understood and modelled. This chapter reviews the different atmospheric contributors to the signal, the formulation of their effect and their relative effects on the measured signal. In particular, the functionality, precision and accuracy of a widely-used radiation transfer code, 5S (Simulation of Satellite Signal in the Solar Spectrum), and its recent successor, 6S (Second Simulation of Satellite Signal in the Solar Spectrum), which enables accurate simulation and correction for atmospheric effects, are examined.

## 1. Introduction

As shown by Tucker in an earlier chapter, the visible and near-infrared channels of the Advanced Very High Resolution Radiometers (AVHRR) onboard the NOAA satellite platforms have proven to be valuable tools for terrestrial applications. However, the signal measured in each of these channels represents a combination of surface and atmospheric effects, usually in different proportions depending on the condition of the atmosphere. Therefore, inherent in any study of the Earth's surface or vegetation from space, is the need to extract the surface contribution from the combined surface/atmosphere reflectance received at the sensor (Deschamps *et al.* 1983, Gordon *et al.* 1988, Justice *et al.* 1991).

This so-called "*decoupling*" of the atmosphere and the surface effect, is a challenging problem, and in the past the research community has attempted to avoid the need for precise atmospheric correction by developing vegetation indices such as the Normalised Difference Vegetation Index (NDVI) (Tucker 1979) which significantly reduces the atmospheric effect due to the normalisation involved in its calculation (Kaufman and Tanré 1992). Further reduction of atmospheric effects, such as those caused by dense haze and sub-pixel-sized clouds, is achieved by the adoption of compositing techniques in which several consecutive images are examined and the value corresponding to the highest value of vegetation index for each pixel is chosen to represent the "*correct*" value for the time period considered (Holben 1986, Kaufman 1987, Tanré *et al.* 1992).



*G. D'Souza et al. (eds.), Advances in the Use of NOAA AVHRR Data for Land Applications,* 49–72.

As well as these pragmatic methods for the removal of unwanted atmospheric effects, there have also been attempts to perform more explicit atmospheric correction by using radiative transfer codes (Moran *et al.* 1990). When such codes are used in conjunction with field measurements of atmospheric optical depth made on the day of satellite overpass, quite accurate atmospheric corrections are possible (Moran *et al.* 1992). However, the acquisition of regular sun-photometer data everywhere is clearly an impossibility. Therefore, simplified methods rely on assumptions, or simulations, of atmospheric conditions, with varying degrees of accuracy (Dozier 1981, Otterman and Fraser 1976, Singh 1988). A major difficulty with these methods is that the highly spatially and temporally variable distribution of the major interfering atmospheric constituents, aerosols and water vapour, cannot be adequately dealt with. Alternatively, and optimally, information about the atmospheric optical properties should be acquired from the satellite scene itself, and combined with suitable radiative transfer models to perform accurate surface/atmospheric decoupling and atmospheric correction. Some methods for the determination of aerosol optical depth directly from the satellite imagery have been developed (Kaufman and Sendra 1988, Holben *et al.* 1992), though these are not yet validated over all terrestrial surfaces.

The need to understand and model the various elements of radiative transfer through the atmosphere as accurately as possible, is obvious. In this chapter we describe various elements of radiative transfer in the wavelength regions of the first two channels of the AVHRR, with reference to one of the most widely-used models for this purpose, 5S (Simulation of Satellite Signal in the Solar Spectrum) (Tanré *et al.* 1983, 1990, 1992), and especially in comparison with the improvements included in its successor, 6S (Second Simulation of Satellite Signal in the Solar Spectrum).

## 2. Radiative Transfer Modelling: The 5S code

In most cases, only a fraction of the visible and near-infrared light reflected from a target reaches the sensor. The two most responsible atmospheric processes for this are: absorption by gases (when observation bands overlap with gaseous absorption bands) and scattering by aerosols or molecules in the atmosphere. In the simple case of a lambertian, homogeneous target at sea level viewed by a satellite sensor (under zenith angle of view $\theta_v$, azimuth angle of view $\phi_v$) and illuminated by sun ($\theta_s$, $\phi_s$), the reflectance received at the sensor may be written as:

$$\rho^*_{Target}(\theta_s, \theta_v, \phi_s-\phi_v) = Tg(\theta_s, \theta_v)\left[\left(\rho^*_{Rayleigh} + \rho^*_{aerosols}\right) + T^{\downarrow}(\theta_s)T^{\uparrow}(\theta_v)\frac{\rho_{Target}}{1 - S\rho_{Target}}\right] \quad (1)$$

Where Tg is the gaseous transmission (in the visible and infrared atmospheric window) and $H_20$, $CO_2$, $O_2$ and $O_3$ are the principal absorbing gases. Over a simple black target, the intrinsic atmospheric reflectance observed, ($\rho^*_{\text{Rayleigh}} + \rho^*_{\text{aerosols}}$) is written here as the

simple sum of reflectance of aerosols and Rayleigh contributions. This simplification, however, is not valid at short wavelengths (less than 0.45 μm) or large sun and view zenith angles (Deschamps *et al.* 1983). The transmission, Tg, is a non-linear function of the effective amount of absorbers in the atmosphere, dependent on the pressure and temperature profiles. In the 5S code this term is computed by a two-band absorption model.

As well as consideration of absorption by atmospheric gases, the 5S code includes routines for a detailed treatment of the scattering process (considering all possible scattering processes along the sun-target-sensor path) and an approximation for the interaction between the absorption and scattering processes (Tanré *et al.* 1992). Since its publication and widespread distribution, the 5S code has been quite widely used in decoupling surface/atmosphere reflectance and atmospheric correction routines. Its success however, has been limited, largely because of a number of shortcomings: the imprecision with which it deals with Rayleigh and aerosol scattering; the limited nature of its inherent spectroscopic data; and it makes no correction for variations in altitude for both sensor and target. Moreover, the assumption of a target with fully lambertian behaviour is a major limitation to its successful application.

In 6S the code accuracy has been improved by addressing all of these specific issues separately. First, the atmospheric reflectance transmission function and spherical albedo aspects of Rayleigh scattering were considered in more detail along with the effects of aerosols, and improvements were also made to the 5S spectroscopic data. Second, the problem of variable altitude for both sensor and target was addressed. Third, bidirectional effects were incorporated with large improvements in the resulting accuracy of the model over the one using the lambertian assumption. In the next sections we provide details concerning the modifications made to 5S that result in the new, improved 6S code, and provide measures of the likely improvements in accuracy and precision.

## 3. The 6S Modifications: Code improvements

### 3.1. RAYLEIGH

3.1.1. *Atmospheric Reflectance.* One of the first improvements to consider in the 6S code (over the 5S version), is concerned with the treatment of atmospheric reflectance. For isotropic scattering Chandrasekhar (1960) showed how solutions derived for small optical thicknesses may be extended to larger values of optical thickness, $\tau$. He expressed the atmospheric reflectance

$$\rho^a(\mu_s,\mu_v,\phi_v-\phi_s)$$

as:

$$\rho_1^a(\mu_s,\mu_v,\phi_v-\phi_s) = \rho_1^a(\mu_s,\mu_v,\phi_v-\phi_s) + (1-e^{-\tau/\mu_s})(1-e^{-\tau/\mu_s})\,\Delta(\tau) \qquad (2)$$

where:

$$\rho_1^a(\mu_s,\mu_v,\phi_v-\phi_s)$$

is the single-scattering contribution and the second term accounts roughly for higher orders of scattering.

In 6S, we used this approach to compute the molecular scattering reflectance (Vermote and Tanré 1992). This molecular reflectance is shown plotted versus the reflectance computed from the successive order of scattering method (see section 3.2) for $\tau = 0.35$ in Figure 1. Four values of the solar zenith angle (0°, 53°, 66° and 70°), 17 values of the viewing zenith angle (from 0° to 60° with a step of 3.3°) and 19 values of the difference of the azimuth angles (from 0° to 180° with a step of 10°), covering a large range of possible geometrical conditions, have been selected. As can be seen, most points fall on the 45-degree line. The right-hand scale, which gives absolute differences between the two results, shows clearly that the precision of 0.001 is achieved for the full range of geometric conditions.

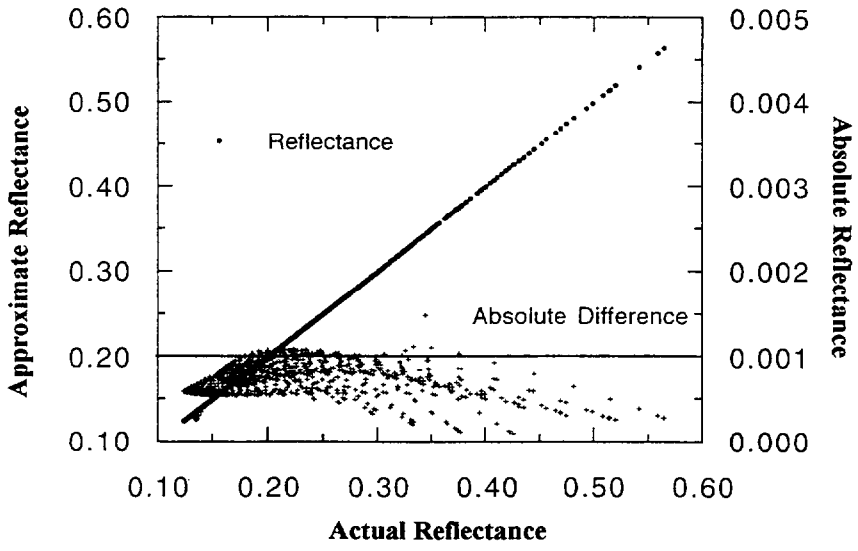


Figure 1. Molecular reflectance versus successive-order-of-scattering reflectance and absolute differences between the two methods for several geometrical conditions with $\tau = 0.35$.

3.1.2. *Transmission Function.* The transmission function refers to the normalised flux measured at the surface. There are several approximate expressions (Joseph *et al.* 1976, Lenoble 1977, Zdunkowski *et al.* 1980) based on the two-stream methods for computing the transmitted flux. The accuracy of these expressions depends on the scattering properties of the atmospheric layer (thick or thin clouds or aerosols) and on the geometrical conditions. The delta-Eddington method (Joseph *et al.* 1976) proved to be well suited for our purposes, and was therefore selected for inclusion in the code. Since molecular scattering is conservative ($\omega_0 = 1$) and the anisotropy factor g is equal to zero, we may write:

$$T(\mu) = \frac{[(2/3) + \mu] + [(2/3) - \mu]e^{-\tau/\mu}}{(4/3) + \tau}, \tag{3}$$

where $\mu$ is the cosine of the solar and/or observational zenith angle and $\tau$ is the optical thickness.

Figure 2 shows a similar comparison as that in Figure 1, this time for the transmission function Equation (3) for four optical thicknesses (0.05, 0.10, 0.25 and 0.35). For the largest optical thickness, the accuracy remains adequate even for very low observation and/or sun angles of 70° for example. The maximum difference is around 0.005, which means a relative accuracy of better than 0.1%.

3.1.3. *Spherical Albedo.* In conservative cases such as molecular scattering, the spherical albedo s is given by:

$$s = 1 - \int_0^1 \mu T(\mu) d\mu \tag{4}$$

where $T(\mu)$ has been given in Equation (3) above. Using Equations (3) and (4), the spherical albedo can be written as:

$$s = \frac{1}{4 + 3\tau} [3\tau - 4E_3(\tau) + 6E_4(\tau)], \tag{5}$$

where $E_3(\tau)$ and $E_4(\tau)$ are exponential integrals for the argument $\tau$. These functions are easily computable from expressions given in the "Handbook of Mathematical Functions" (Abramowitz and Stegun 1970).

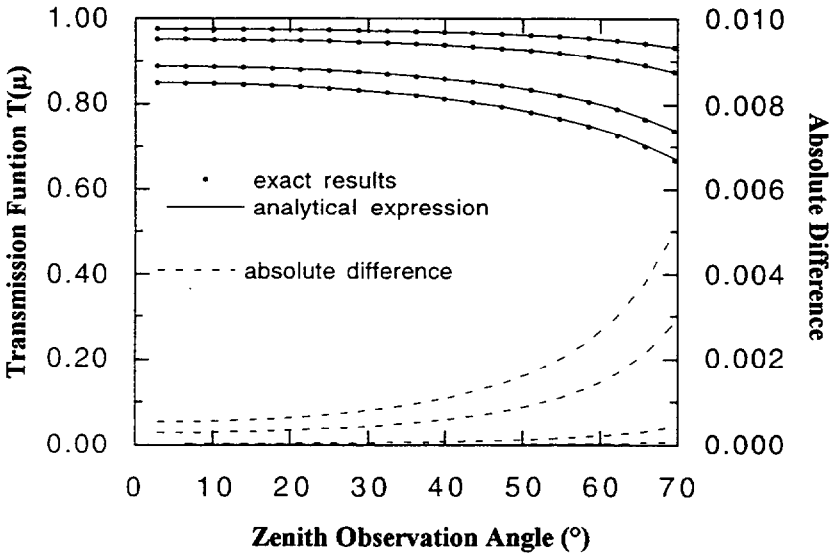


Figure 2. Comparison between actual transmission function and the delta-Eddington approximation used in 6S.

Figure 3 shows results of the expression for the spherical albedo, s. The differences between the exact results and Equation (5) are around only 0.003 for $\tau = 0.35$ which results in an error of only 0.0003 for a surface albedo of 0.10. In the red part of the solar spectrum for which the surface albedo may be larger, the error is still below 0.002.

### 3.2. AEROSOL

Sobolev's (1975) approximation for the reflectance, Zdunkowsky's method (1980) for the transmittance, and a semi-empirical formula for the spherical albedo. The advantage of this was that users with limited computing resources could still obtain approximations quickly. The drawback was that the accuracy of the computations could be inaccurate by a few percent in reflectance units, especially at large view and sun angles and high optical thickness. In addition, these approximations could be completely inadequate for handling the integration of the downward radiance field with non-lambertian ground conditions, typically the problem of bidirectional reflectance distribution function (BRDF) simulation. The new scheme of computation where aerosol plus Rayleigh contributions are treated as a coupled system relies on the "Successive Order of Scattering" method used by several authors (*e.g.* Ahmad and Fraser 1982, Deuzé *et al.* 1989). The accuracy of such a scheme is better than $2 \times 10^{-4}$ reflectance units.

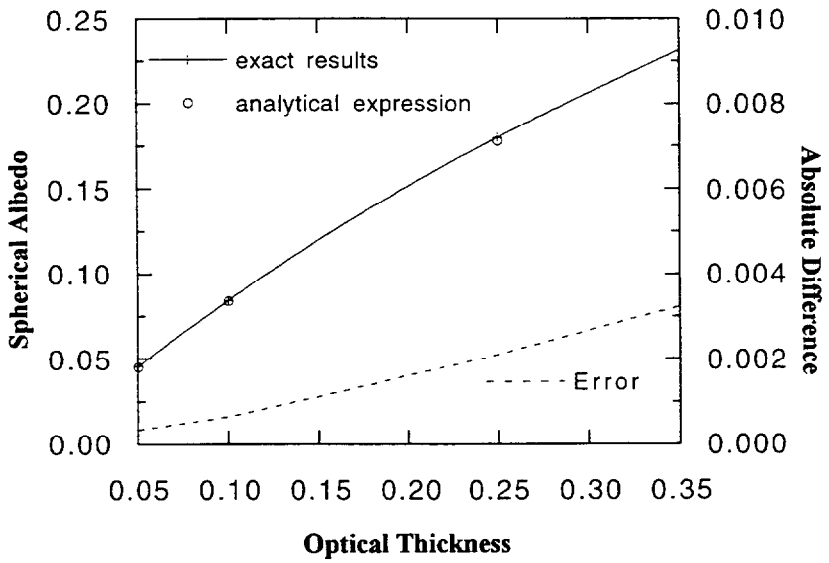


Figure 3. Comparison between actual spherical albedo and the approximation used in 6S.

In our application, the atmosphere is divided into 13 layers, which enables exact simulations of airborne observations. The downward radiation field is also computed for a quadrature of 13 gauss emerging angles which provides the necessary inputs for BRDF simulations (see section 5). The computing time remains reasonable and is in the order of only a few seconds on an HP735 Workstation (approximately 124 MIPS).

### 3.3. SPECTROSCOPIC DATA

In relation to spectroscopy, the computation scheme used in 5S has not been changed, but the accuracy and resolution of the spectroscopic data have been improved. The spectral resolution of 6S has been improved to 10 $cm^{-1}$ with respect to band absorption models - the data having been generated using the HITRAN database. Also, $CH_4$,CO and $NO_2$ are now taken into account in the computation of the gaseous transmission. The computation of the water vapour absorption has also been improved according to recent findings, and differences between 5S and 6S values can reach a few percent for this term. Figures 4a-c show that the 6S computations match very well those obtained by MODTRAN (5 $cm^{-1}$ resolution) in the example of the typical US62 atmosphere.

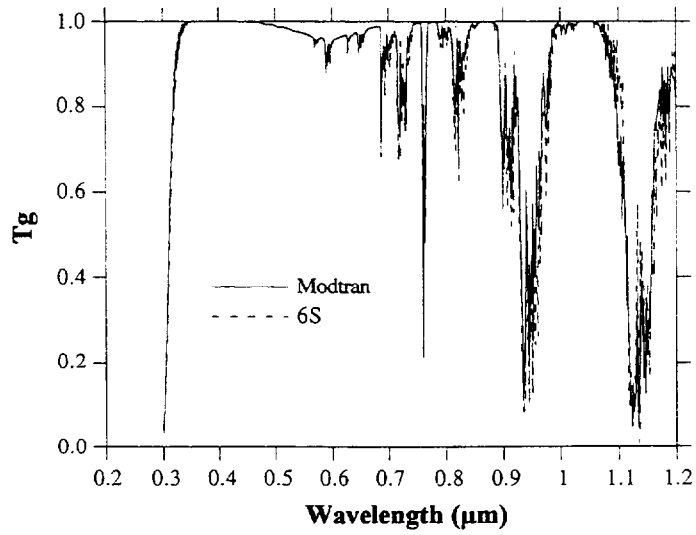


Figure 4a. Comparison of gaseous transmission as computed by MODTRAN and 6S for a typical US62 atmosphere between 0.20 and 1.20 μm.

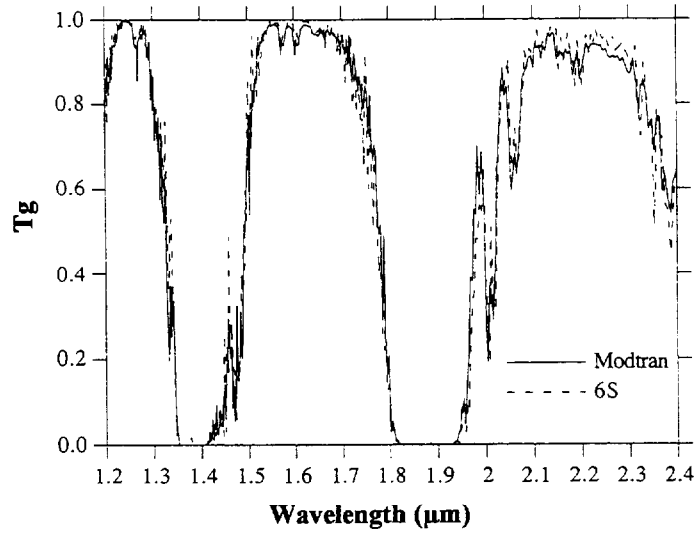


Figure 4b. Comparison of gaseous transmission as computed by MODTRAN and 6S for a typical US62 atmosphere between 1.20 and 2.40 μm.

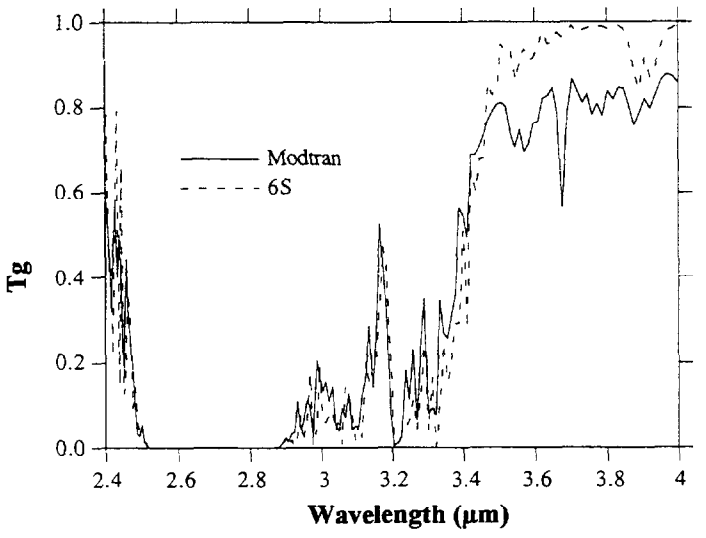


Figure 4c. Comparison of gaseous transmission as computed by MODTRAN and 6S for a typical US62 atmosphere between 2.40 and 4.0 µm.

## 4. The 6S Modifications: target and sensor altitude

### 4.1. ELEVATED TARGET SIMULATION

Where targets are above sea level, Equation 1 may be modified as follows:

$$\rho^{*}_{\text{Target}}(\theta_s, \theta_v, \phi_s\text{-}\phi_v, z_t) =$$

$$\text{Tg}(\theta_s, \theta_v, z_t)\left[\rho^{*}_{\text{Rayleigh}}(z_t) + \rho^{*}_{\text{aerosols}} + \text{T}^{\Uparrow}(\theta_v, z_t)\text{T}^{\Downarrow}(\theta_s, z_t)\frac{\rho_{Target}}{1 - \text{S}(z_t)\rho_{Target}}\right], \qquad (6)$$

where $z_t$ is the target altitude.

The target altitude and pressure indicates the amount of scatterers above the target (molecules and aerosols) and the amount of gaseous absorbents. In the 5S code, the amount and type of aerosol is entered as a fixed parameter, thus the aerosol characteristics implicitly depend on target altitude because these are measured at target location. For 6S the target altitude is handled in the following manner: first the atmospheric profile and the target altitude or pressure is selected, then a new atmospheric profile is computed by stripping out the atmospheric level above target altitude and interpolating if necessary. In

this way, a more precise computation of the atmospheric parameters is made, without any kind of approximation and taking into account the coupled pressure-temperature effect on absorption. In most cases, only the integrated content may be modified as already pointed out by Teillet and Santer (1991). The user still has the option to enter the total amount of $H_2O$ and $O_3$, but in this case the quantity entered must be representative of the level measured or estimated at the target location.

The influence of target altitude on Tg for an observation made with solar zenith angle, $\theta_s$ = 30° and view zenith angle $\theta_v$ = 60°, is shown in Figure 5. As can be seen, the absorption effect of $O_3$ is not sensitive to altitude target, because the ozone layer is located in the upper levels of the atmosphere. However, target altitude does have an important effect on absorption by $H_2O$ as the models show. This is because most of the water vapour is located in the lower atmosphere, although it should be noted that the water vapour profile in the atmosphere is highly variable.

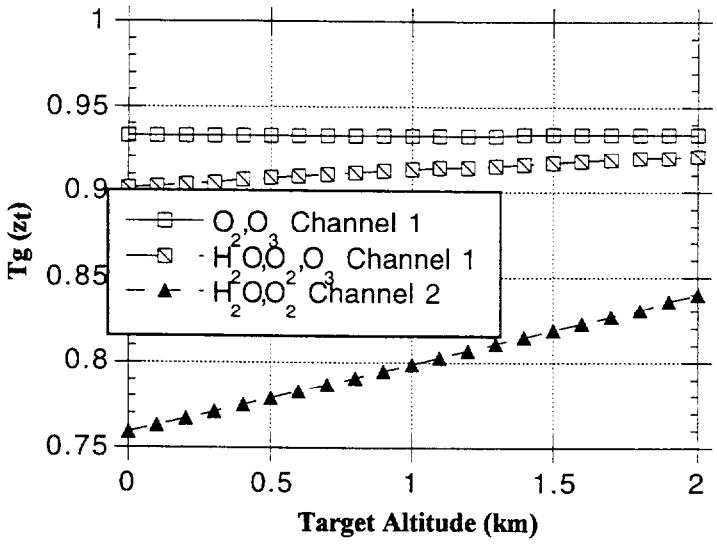


Figure 5. The influence of target altitude on the transmission function, Tg.

The effect of target altitude on molecular optical thickness is also accounted for precisely in 6S. A good approximation, however, is to consider that $\tau_R$ is proportional to the pressure at target level. Figure 6, compares, for the case of observation in AVHRR channel 1, the exact computation (derived from modified Mid-latitude Summer profile) to the approximation $\tau_R$ proportional to pressure ($z_{target}$).

Figure 7 illustrates the influence of altitude target, in terms of absolute variation of the Rayleigh reflectance for AVHRR channel 1 for the whole globe, using the 1/3 of degree resolution elevation map. For each 1/3 x 1/3 degree cell, considering a constant view angle of 30°, a map has been computed for solar zenith angle of 30° (backscattering). The Digital Elevation Model used in this simulation is ETOPO5. The error made by neglecting the target altitude in Rayleigh correction can reach 0.016 reflectance units but is usually between 0.001 and 0.01 for most cases.

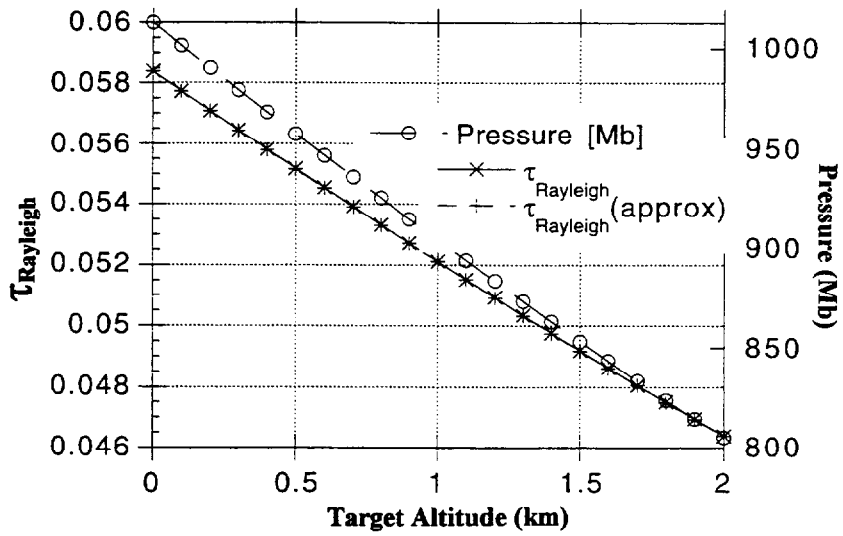


Figure 6. The effect of target altitude on molecular optical thickness as approximated in 6S.

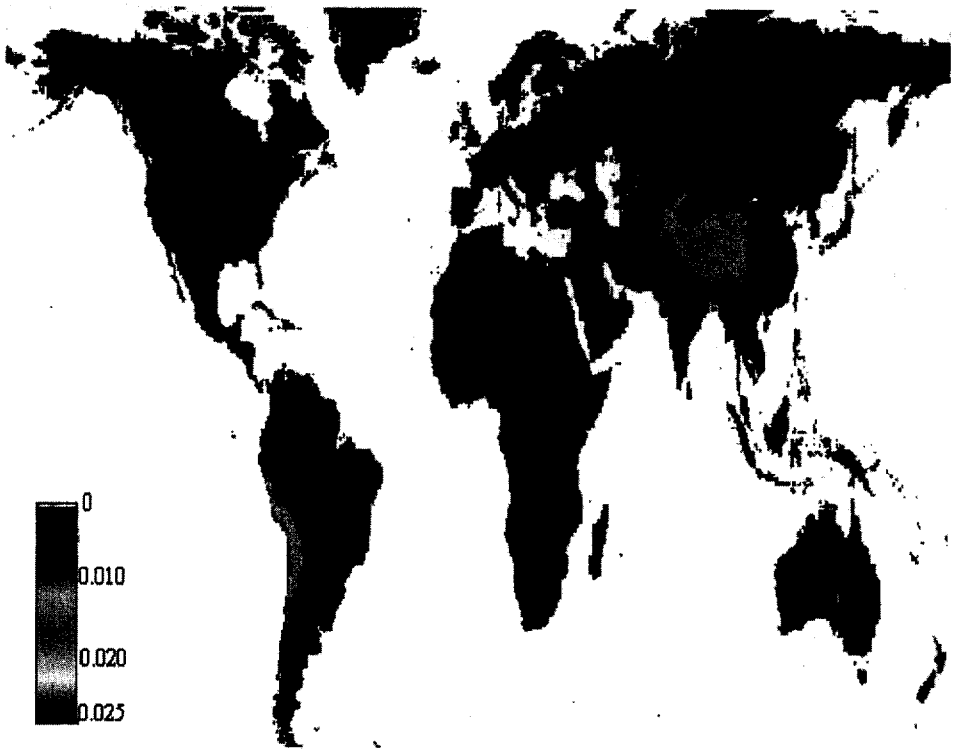


Figure 7. Absolute variation of Rayleigh reflectance for channel 1 of AVHRR due to ground altitude variation. The digital elevation model used for altitude is ETOPO5.

## 4.2. AIRBORNE SENSOR SIMULATION

4.2.1. *Gaseous Absorption.* When a sensor is inside the atmosphere (as is the case with airborne sensors), Equation (1) is modified as follows:

$$\rho^{*}_{Target}\,(\theta_s, \theta_v, \phi_s\text{-}\phi_v, z) =$$

$$\mathrm{Tg}\,(\theta_s, \theta_v, z)\,[\rho^{*}_{Rayleigh}\,(z) + \rho^{*}_{aerosols}(z) + \mathrm{T}^{\uparrow}(\theta_v, z)\mathrm{T}^{\downarrow}(\theta_s, z)\frac{\rho_{Target}}{1 - \mathrm{S}(z_t)\,\rho_{Target}}], \qquad (7)$$

In this case gaseous absorption is computed using a technique similar to that used for targets above sea level. The upward path only is modified: the atmosphere level above the sensor altitude is stripped, so computation is carried out only to the altitude of the sensor (with interpolation of the atmospheric profile as necessary). Figure 8 illustrates the effect of altitude on gaseous transmission computation, for $\theta_s = 30°$, $\theta_v = 60°$. In the case of the spectral wavelength of AVHRR's visible channel, $O_3$ absorption along the target-sensor path is no longer taken into account because these molecules are only located above the airborne sensor. For $H_2O$, absorption is highly dependent on altitudes up to 4 km. Thus, if the observed channel is sensitive to water vapour absorption (as is the case with AVHRR channel 2) we recommend that additional measurements of water vapour should be taken from the aircraft. An additional option has been set up in 6S for this purpose and enables

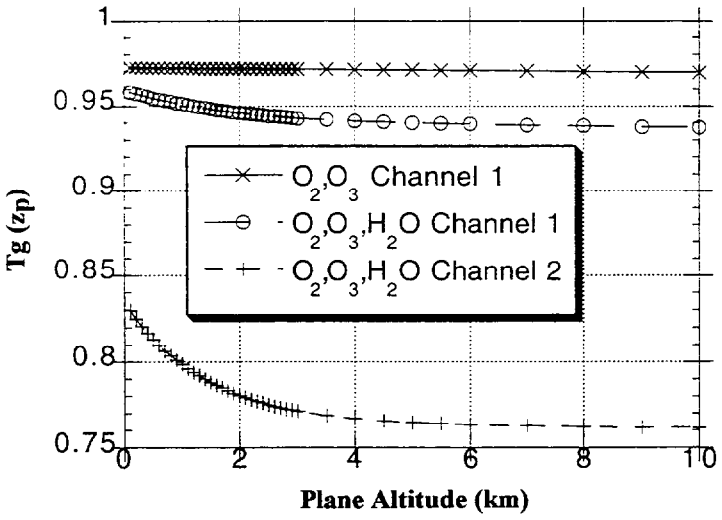


Figure 8. The effect of altitude on gaseous transmission computation for $\theta_s = 30°$ and $\theta_v = 60°$.

the user to enter aerosol, ozone and water vapour content for the portion of the atmosphere located under the aircraft if these are known or can be calculated.

4.2.2. *Atmospheric Reflectance and Transmittance.* In most cases the simple approximation "equivalent atmosphere", for atmospheric reflectance and transmittance is sufficiently accurate, *i.e*:

$$\rho^{*}_{Rayleigh}(z) \cong \rho^{*}_{Rayleigh}(z = \infty,\ \tau_R(0 \rightarrow z)) \tag{8}$$

$$T^{\uparrow}(\tau_R, \theta_v, z) \cong T^{\uparrow}(\tau_R(0 \rightarrow z),\ \theta_v, z = \infty) \tag{9}$$

In Figures 9 and 10 we present the comparison between approximations using Equation (8) and (9) and exact computation, provided by a radiative code, again based on the Successive Order of Scattering method. As can be seen, the approximations work very well with only small absolute differences.

However, at wavelengths less than 550 nm, as can be seen in Figure 11, the accuracy of Equation 8 is not as good in the case of a mixed Rayleigh-aerosol atmosphere. Therefore, in 6S, the computation is performed exactly by defining one of the multiple layers used in the Successive Order of Scattering at the altitude of the sensor. This enables exact computation of both reflectance and transmission term for a realistic mixing between aerosol and Rayleigh components.

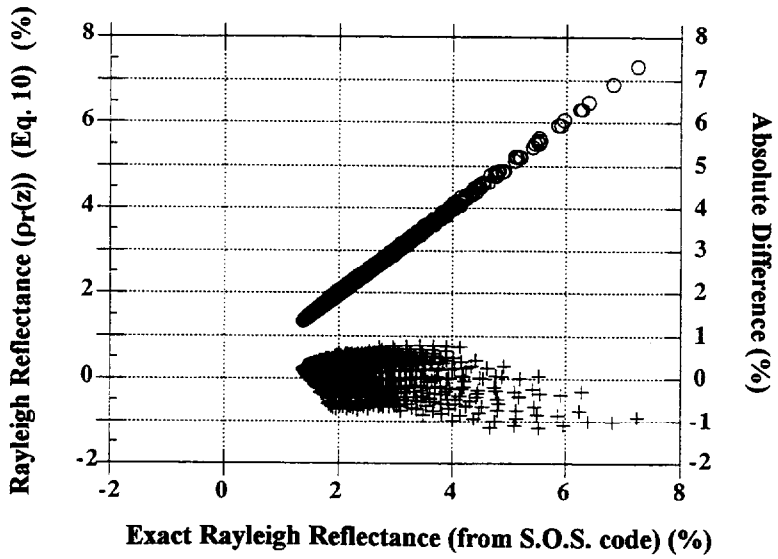


Figure 9. Atmospheric Rayleigh reflectance approximation (Equation 8) as used in 6S versus exact Rayleigh reflectance calculated using the Successive Order of Scattering (S.O.S.) code.

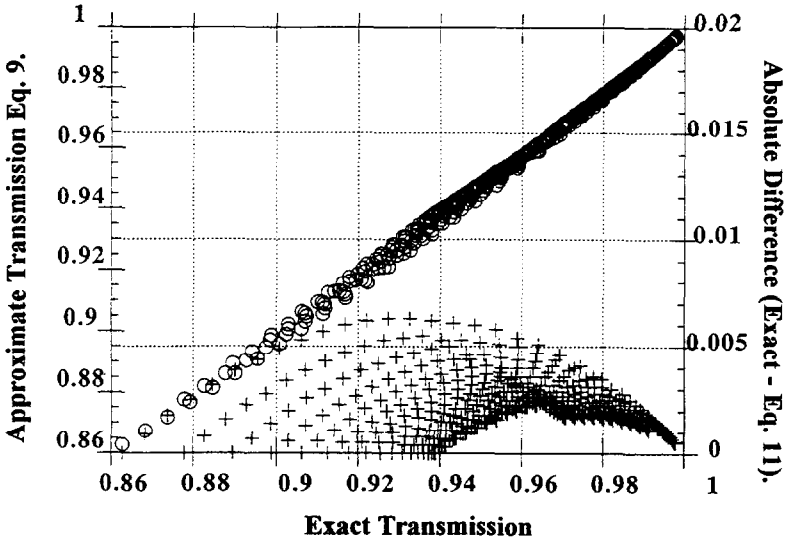


Figure 10. Atmospheric transmission approximation (Equation 9) as used in 6S versus exact transmission calculated using the Successive Order of Scattering (S.O.S.) code

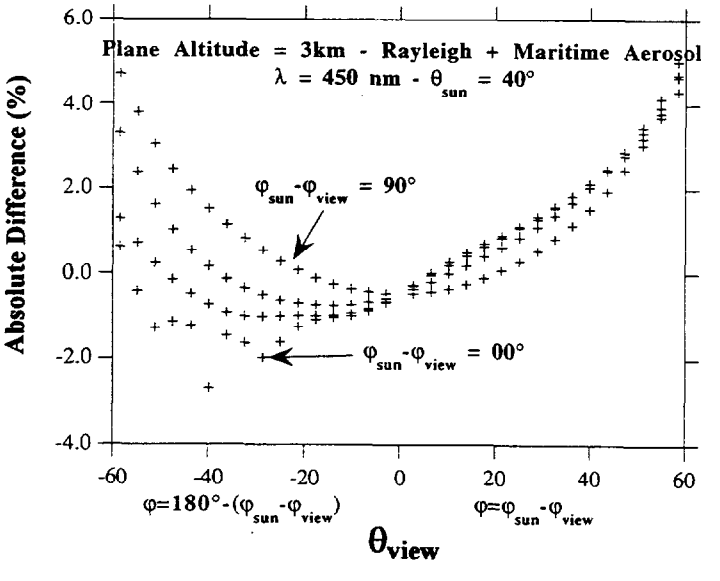


Figure 11. Comparison of Rayleigh reflectances between approximation (Equation 8) and exact computation at 450 nm in case of a moderate maritime aerosol background (Visibility of 23 km).

## 4.3. NON-HOMOGENEOUS TARGET

In the case of non-homogeneous targets the approach adopted in 5S is to write the signal at the Top of The Atmosphere as:

$$\rho^*_{Target}(\theta_s,\theta_v,\phi_s-\phi_v)=\mathrm{Tg}(\rho^*_{atm}+\mathrm{T}^{\Downarrow}(\theta_s)(\rho_{Target}e^{-\tau/\mu_v}+t_d(\vartheta_v))\frac{<\rho>}{1-S(z)<\rho>}) \quad (10)$$

where:

$$<\rho> = F(r)\,\rho_{Target} + (1\text{-}F(r))\rho_{env} \quad (11)$$

and the environment function $F(r)$ is given by:

$$F(r) = \frac{t_d^R(\mu_v)F_R(r)+t_d^A(\mu_v)F_A(r)}{t_d(\mu_v)} \quad (12)$$

If we consider target and environment to be at the same altitude, the problem of a target above sea level can be solved just by modifying the Rayleigh optical thickness.

In the case of aircraft observations, however, we have to first take into account reduction of the amount of scatterers under the aircraft. This can be done just by adjusting the term,

$$t_d^R(\mu_v)F_R(r) \text{ to } t_d^R(z,\mu_v)t_d^A(z,\mu_v)$$

Once this has been done the principal part of the effect is taken into account, that is, a global reduction (a factor of 5-10 for a flying height of 6 km) of the "environment effect". The second effect is the dependence of $F_R(r)$ and $F_A(r)$ upon sensor altitude. Monte Carlo simulations of $F_R(r)$ and $F_A(r)$ have been performed for sensor altitudes between 0.5 and 12 km and included in 6S as a database (see Figures 12-13). In the case of aircraft observation, the closest simulated altitudes are used to interpolate the environment function at the aircraft altitude.

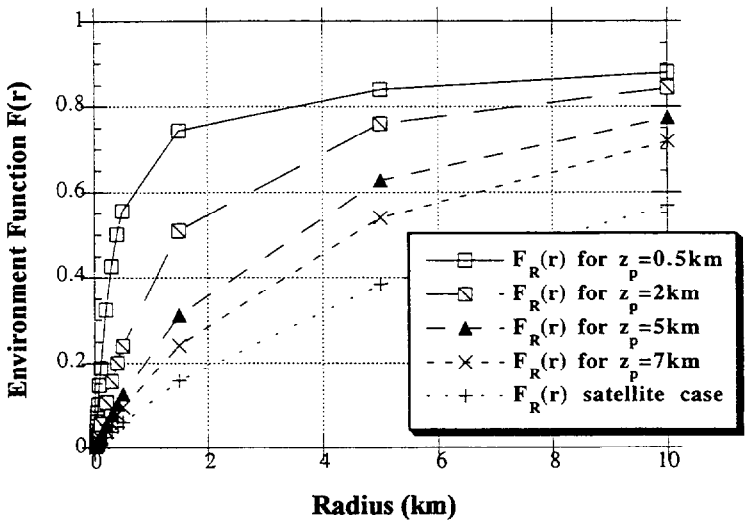


Figure 12. Variation of the environment functions, Rayleigh ($F_R$) for different altitudes of the sensor.

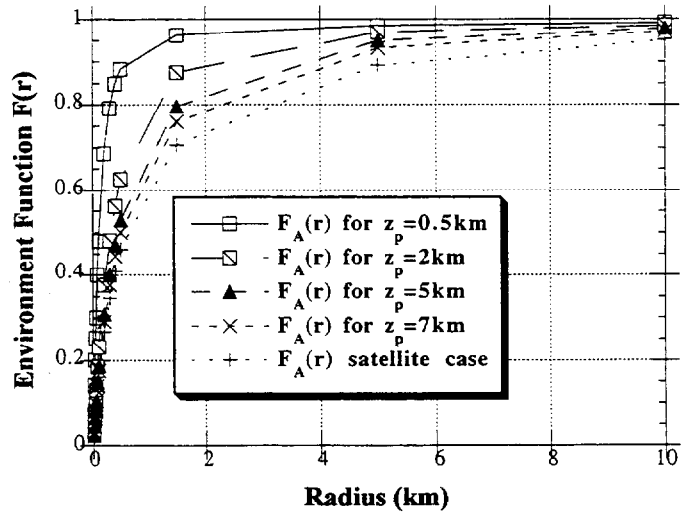


Figure 13. Variation of the environment functions for aerosol ($F_A$) for different altitudes of the sensor.

## 5. The 6S modifications: bidirectional reflectance distribution function (BRDF)

### 5.1. THEORETICAL BACKGROUND

In 6S, the coupling BRDF atmosphere is taken into account according to the scheme presented in Tanré *et al.* (1986). The contribution of the target to the signal at the top of the atmosphere is assumed to be the sum of four terms: (a) the photons directly transmitted from the sun to the target and directly reflected back to the sensor, (b) the photons directly transmitted to the target but scattered by the atmosphere on their way to the sensor, (c) the photons scattered by the atmosphere then reflected by the target and directly transmitted to the sensor, and finally, (d) the photons having at least two interactions with the atmosphere. The exact contribution of a-d is according to the following set of Equations (13a-d) as already shown in Tanré *et al* (1983).

$$e^{-\tau/\mu_s}\,\rho(\mu_s,\mu_v,\phi)\,e^{-\tau/\mu_v} \tag{13a}$$

$$t_d(\mu_s)\,\overline{\rho}(\mu_s,\mu_v,\phi)\,e^{-\tau/\mu_v} = t_d(\mu_s)\frac{\int_0^{2\pi}\int_0^1 \mu L^{\Downarrow}(\mu_s,\mu_v,\phi')\,\rho(\mu,\mu_v,\phi'-\phi)\,d\mu\,d\phi}{\int_0^{2\pi}\int_0^1 \mu L^{\Downarrow}(\mu_s,\mu,\phi')\,d\mu\,d\phi}\,e^{-\tau/\mu_v} \tag{13b}$$

$$t_d(\mu_v)\,\overline{\rho}'(\mu_s,\mu_v,\phi)\,e^{-\tau/\mu_s} = t_d(\mu_v)\,\overline{\rho}(\mu_v,\mu_s,\phi)\,e^{-\tau/\mu_s} \tag{13c}$$

$$t_d(\mu_v)t_d(\mu_s)\overline{\overline{\rho}} = t_d(\mu_v)t_d(\mu_s)\,\rho''(\mu_s,\mu_v,\phi), \tag{13d}$$

where

$$\overline{\overline{\rho}} \cong \int_0^1 \mu_s \int_0^{2\pi}\int_0^1 \mu_v\,\rho(\mu_s,\mu_v,\phi'-\phi)\,d\mu_v\,d\phi\,d\mu_s \tag{13e}$$

In 6S, the first three contributions are computed exactly using a downward radiation field as obtained by the successive order of scattering method. The fourth contribution which involves at least two interactions between the atmosphere and the BRDF

(Equations 13d and e) is approximated by taking $\bar{\bar{\rho}}$ equal to the hemispherical albedo of the target. This approximation is necessary because the exact computation would require a double integration, and it is justified by the limited impact on the total signal of this last contribution relative to $t_d(\mu_v)t_d(\mu_s)$, and also because multiple scattering tends to be isotropic.

## 5.2. VALIDATION

Thus, the only approximation in the computing scheme of 6S for BRDF effects is in the estimation of multiple interaction between target and atmosphere. Figure 14 shows that the effect of this approximation is only small for a typical BRDF signature, the clover patch measured by Woessner and Hapke (1987), and Figure 15 shows that the approximation works quite well in a range of condition as compared with the results obtained from the Successive Order of Scattering method. The ground BRDF in the example is from Kime's measurements over a ploughed field fitted with the Hapke BRDF model.

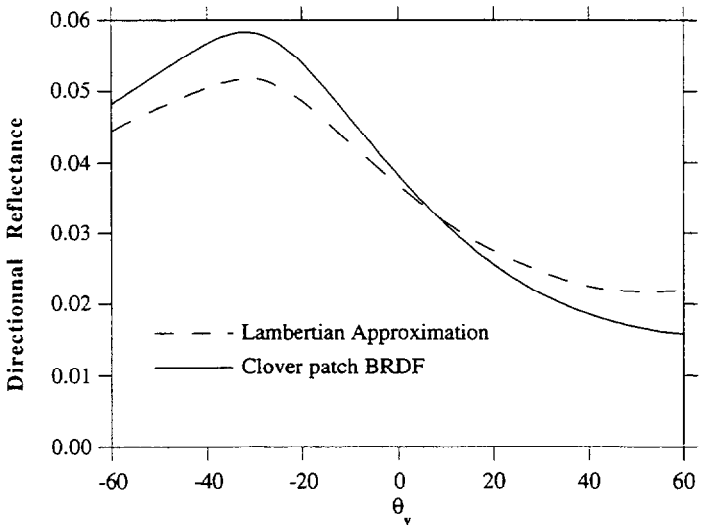


Figure 14. Comparison of the exact signal with the approximation given by Equation 13d. The target is a clover patch at 450 nm, the atmosphere is clear (visibility of 100 km) and the solar zenith angle is 30 degrees.

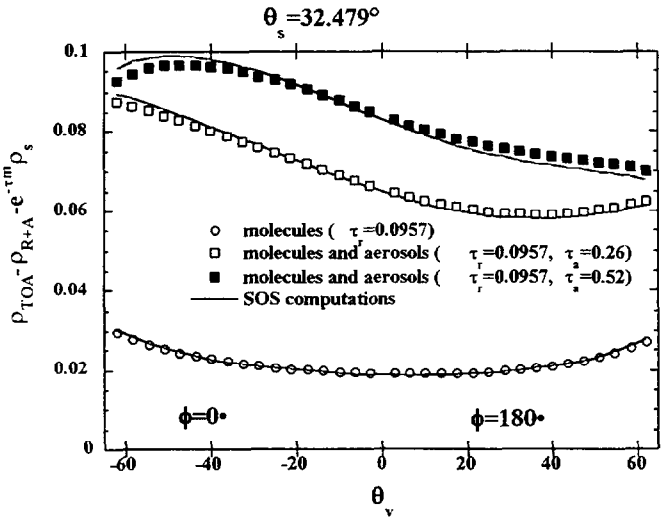


Figure 15 Comparison of the sum of the coupling terms atmosphere-BRDF: $\rho_{TOA} - (\rho_{...} - e^{-\tau m}\rho_s)$; computed by 6S with the same quantity computed by the Successive Order of Scattering code for different atmospheric conditions (clear, average, turbid). The ground BRDF is from Kime's measurements over a ploughed field fitted with the Hapke BRDF model

## 6. Conclusions

Modifications and significant improvements, both in terms of accuracy and in application, have been made to the 5S radiative transfer code, to produce a new version, 6S. Although some parts of the new code are highly sophisticated, the computation time remains reasonable, and the input parameters and the structure of the code remain very similar to the 5S version, so that existing users may make the transition easily to 6S.

The use of 6S for precise radiometric calibration and atmospheric correction will be illustrated in the following chapters.

## Glossary

| | |
|---|---|
| $\theta_S$ | Solar zenith angle |
| $\mu_S$ | Cosine of solar zenith angle |
| $\theta_V$ | View zenith angle |
| $\mu_S$ | Cosine of view zenith angle |
| $\phi_S$ | Solar azimuth angle |
| $\phi_V$ | View azimuth angle |
| $\rho$ | reflectance (unitless) |
| Tg | gaseous transmission |
| T | total scattering transmission (diffuse+direct) |
| $t_d$ | diffuse transmittance factor |
| $\tau$ | optical thickness (unitless) |
| s | spherical albedo |
| z | altitude of the target |
| $\mu$m | micrometer |
| F(r) | environment function |

## References and Bibliography


Abel, P., Guenther, B., Galimore, R. N. and Cooper, J. W., 1993, Calibration Results for NOAA-11 AVHRR Channels 1 and 2 from Congruent Path Aircraft observations. *Journal of Atmospheric and Oceanic Technology,* **10,** 4, 493-508.

Abramowitz, M. and Stegun, I., A, 1970, *Handbook of Mathematical Functions* (New-York: Dover Publications,Inc).

Ahmad, Z. and Fraser, R. S., 1982, An iterative radiative transfer code for ocean-atmosphere system. *Journal of Atmospheric Science,* **39,** 656-665.

Brest, C. L. and Rossow, W. L., 1991, Radiometric calibration and monitoring of NOAA AVHRR data for ISCCP. *International Journal of Remote Sensing,* **13,** 235-273.

Chandrasekhar, S., 1960, *Radiative Transfer* (Dover: New York).

Che, N. and Price, J. C., 1992, Survey of Radiometric Calibration Results and Methods for Visible and Near Infrared Channels of NOAA-7,-9, and -11 AVHRR's. *Remote Sensing of Environment,* **41,** 19-27.

Cox, C. and Munk, W., 1965, Slopes of the sea surface deduced from photographs of sun glitter. *Bulletin of Scripps Institute of Oceanography of University of California,* **6,** 401-488.

Deschamps, P. Y., Herman, M. and Tanré, D., 1983, Modeling of the atmospheric effects and its application to the remote sensing of ocean color. *Applied Optics,* **22,** 23, 3751-3758.

Deuzé, J. L., Herman, M. and Santer, R., 1989, Fourier series expansion of the transfer equation in the atmosphere-ocean system. *Journal of Quantitative Spectroscopy and Radiative Transfer*, **41**, 6, 483-494.

Dozier, J., 1981, A method for satellite identification of surface temperature fields of subpixel resolution. *Remote Sensing of Environment*, **11**, 221-229.

Fraser, R. S. and Kaufman, Y. J., 1986, Calibration of satellite sensors after launch. *Applied Optics*, **25**, 1177-1185.

Frouin, R. and Gautier, C., 1987, Calibration of NOAA-7 AVHRR, GOES-5 and GOES-6 VISSR/VAS solar channels. *Remote Sensing Environment*, **22**, 73-101.

Gordon, H. R., Brown, J. W. and Evans, R. H., 1988, Exact Rayleigh scattering calculations for use with the Nimbus-7 Coastal Zone Color Scanner. *Applied Optics*, **27**, 5, 862-871.

Holben, B. N., 1986, Characteristics of maximum-value composite images for temporal AVHRR data. *International Journal of Remote Sensing*, **7**, 11, 1435-1445.

Holben, B. N., Kaufman, Y. J. and Kendall, J. D., 1990, NOAA-11 AVHRR visible and near-IR inflight calibration. *International Journal of Remote Sensing*, **11**, 8, 1511-1519.

Holben, B. N., Vermote, E., Kaufman, Y. J., Tanré, D. and Kalb, V., 1992, Aerosol retrieval over Land from AVHRR data-application for atmospheric correction. *IEEE Transaction on Geoscience and Remote Sensing*, **30**, 2, 212-222.

Joseph, J. H., Wiscombe, W. J. and Weinman, J. A., 1976, Solar Flux Transfer Through Turbid Atmospheres Evaluated by the Delta-Eddington Approximation. *Journal of Atmospheric Science*, **33**, 2452-2459.

Justice, C. O., Eck, T. F., Tanré, D. and Holben, B. N., 1991, The effect of water vapour on the normalized difference vegetation index derived for the Sahelian region from NOAA AVHRR data. *International Journal of Remote Sensing*, **12**, 6, 1165-1187.

Kaufman, Y., J, 1987, The effect of subpixel cloud on remote sensing. *International Journal of Remote Sensing*, **8**, 839-856.

Kaufman, Y. J. and Holben, B. N., 1993, Calibration of the AVHRR visible and near-IR bands by atmospheric scattering, ocean glint and desert reflection. *International Journal of Remote Sensing*, **14**, 21-52.

Kaufman, Y. J. and Sendra, C., 1988, Algorithm for automatic atmospheric corrections to visible and near-IR satellite imagery. *International Journal of Remote Sensing*, **9**, 8, 1357-1381.

Kaufman, Y. J. and Tanré, D., 1992, Atmospherically resistant vegetation index (ARVI) for EOS-MODIS. *IEEE Transactions on Geoscience and Remote Sensing*, **30**, 2, 261-270.

King, M., Harshvardhan, D. and Arking, A., 1984, A model of the radiative properties of the El Chichon Stratospheric Aerosol layer. *Journal of Climate and Applied Meteorology*, **23**, 7, 1121-1137.

Koepke, P., 1982, Vicarious satellite calibration in the solar spectral range by means of calculated radiances and its application to Meteosat. *Applied Optics,* **21,** 15, 2845-2854.

Koepke, P., 1984, Effective reflectance of oceanic white caps. *Applied Optics,* **20,** 24,

Lenoble, J., 1977, Standard procedures to compute Atmospheric Radiative Transfer in a Scattering Atmosphere Radiation Commission, IAMAP, National Center for Atmospheric Research, Boulder,CO,

London, J., Bojkov, D. R., Oltmans, S. and Kelly, J. L., 1976, Atlas of the Global Distribution of the Total Ozone July 1957-June 1967 NCAR/TN/113+STR, NCAR, Boulder, Colorado, USA.

McCormick, M. P. and Veiga, R. E., 1992, SAGE II Measurements of early Pinatubo aerosols. *Geophysical Research letters,* **19,** 2, 155-158.

Mitchell, R. M., O'Brien, D. M. and Forgan, B. W., 1992, Calibration of the NOAA AVHRR Short-wave Channels Using Split Pass Imagery: I. Pilot Study. *Remote Sensing of Environment,* **40,** 57-65.

Moran, M. S., Jackson, R. D., Hart, G. F., Slater, P. N., Bartell, R. J., Biggar, S. F., Gellman, D., I. and Santer, R. P., 1990, Obtaining surface factors from atmospheric and view angle corrected SPOT-1 HRV data. *Remote Sensing of Environment,* **32,** 203-214.

Moran, M. S., Jackson, R. D., Slater, P. N. and Teillet, P. M., 1992, Evaluation of simplified procedures for retrieval of land surface reflectance factors from satellite sensor output. *Remote Sensing of Environment,* **41,** 169-184.

Otterman, J. and Fraser, R., 1976, Earth-atmosphere system and surface reflectivities in arid regions from Landsat MSS data. *Remote Sensing of Environment,* **5,** 247-266.

Price, J. C., 1987, Calibration of satellite radiometers and the comparison of vegetation indexes. *Remote Sensing Environment,* **21,** 15-27.

Price, J. C., 1988, An update on visible and near IR calibration of satellite instruments. *Remote Sensing Environment,* **24,** 419-422.

Singh, S. M., 1988, Simulation of solar zenith angle effect on global vegetation index (GVI) data. *International Journal of Remote Sensing,* **9,** 2, 237-248.

Smith, G. R., Levin, R. H., Abel, P. and Jacobowitz, H., 1988, Calibration of the solar channels of the NOAA-9 AVHRR using high altitude aircraft measurements. *Journal of Atmospheric and Oceanic Technology,* **5,** 631-639.

Sobolev, V. V., 1975, *Light scattering in Planetry Atmospheres*, Pergamon Press, New York.

Staylor, W. F., 1990, Degradation rates of the AVHRR visible channel for the NOAA 6,7 and 9 Spacecraft. *Journal of Atmospheric and Oceanic Technology*, 7, 411-423.

Stowe, L. L., Carey, R. M. and Pellegrino, P. P., 1992, Monitoring the Mt. Pinatubo aerosol layer with NOAA/11 AVHRR data. *Geophysical Research Letter,* **19,** 2, 159-162.

Stowe, L. L., McClain, E. P., Carey, R., Pellegrino, P., Gutman, G. G., Davis, P., Long, C. and Hart, S., 1991, Global Distribution of Cloud Cover derived from

NOAA/AVHRR operational Satellite Data. *Advances in Space Research / COSPAR,* 11 COSPAR), pp. 51-54.

Tanré, D., Herman, M. and Deschamps, P. Y., 1983, Influence of the atmosphere on space measurements of directional properties. *Applied Optics,* **21,** 733-741.

Tanré, D., Deroo, C., Duhaut, P., Herman, M., Morcette, J. J., Perbos, J. and Deschamps, P. Y., 1990, Description of a computer code to simulate the satellite signal in the solar spectrum: 5S code. *International Journal of Remote Sensing,* **11,** 659-668.

Tanré, D., Holben, B. N. and Kaufman, Y. J., 1992, Atmospheric Correction algorithm for NOAA-AVHRR Products: Theory and Application. *IEEE Transaction on Geoscience and Remote Sensing,* **30,** 2, 231-248.

Teillet, P. M. and Santer, R. P., 1991, Altitude dependence in a semi-analytical atmospheric code. *Physical Measurements and Signatures in Remote Sensing, France,* ESA, pp. 36-44.

Teillet, P. M., Slater, P. N., Ding, Y., Santer, R. P., Jackson, R. D. and Moran, M. S., 1990, Three Methods for the Absolute Calibration of the NOAA AVHRR Sensors In-Flight. *Remote Sensing of Environment,* **31,** 105-120.

Tucker, C. J., 1979, Red and photographic infrared linear combinations monitoring vegetation. *Remote Sensing Environment,* **8,** 127-150.

Tucker, C. J., 1986, Maximum normalized difference vegetation index images for sub-Saharan Africa for 1983-1985. *International Journal of Remote Sensing,* **7,** 1383-1384.

Vermote, E., El Saleous, N. and Holben, B. N., 1993, Atmospheric Correction of AVHRR visible and Near Infrared Data. *Workshop on atmospheric correction of Landsat Data.*

Vermote, E., Santer, R., Deschamps, P. Y. and Herman, M., 1992, In-flight calibration of large field of view sensors at short wavelengths using Rayleigh scattering. *International Journal of Remote Sensing,* **13,** 18, 3409-3429.

Vermote, E. F. and Tanré, D., 1992, Analytical Expressions for Radiative Properties of Planar Rayleigh Scattering Media Including Polarization Contribution. *Preprint for Journal Of Quantitative Spectroscopy and Radiative Transfer,* **47,** 4, 305-314.

Whitlock, C. H., Staylor, W. F., Smith, G., Levin, R., Frouin, R., Gautier, C., Teillet, P. M., Slater, P. N., Kaufman, Y. J., Holben, B. N., Rossow, W. B., Brest, C. and LeCroy, S. R., 1988, AVHRR and VISSR satellite instrument calibration results for both cirrus and marine stratocumulus IFO periods. *FIRE Science Team Meeting, Vail, Colorado*

Woessner, P. and Hapke, B., 1987, Polarization of light scattered by clover. *Remote Sensing of Environment,* **21,** 243-261.

Zdunkowski, W. G., Welch, R. M. and Korb, G., 1980, An investigation of the Structure of Typical Two-stream-methods for the Calculation of Solar Fluxes and Heating Rates in Clouds. *Contributions to Atmospheric Physics,* **53,** 2, 147-165.